Check for updates

JGR Solid Earth

RESEARCH ARTICLE
10.1029/2025JB032994

Hindered but Not Halted Crustal Flow: Implications From Lg-Wave Attenuation Tomography Based on High-Density ChinArray in SE Tibetan Plateau

Xi He[1], Lian-Feng Zhao[1,2], Xiao-Bi Xie[3], Ruo-Jie Li[1], Tong Lu[1], and Zhen-Xing Yao[1]

[1]Key Laboratory of Planetary Science and Frontier Technology, Institute of Geology and Geophysics, Chinese Academy of Sciences, Beijing, China, [2]Heilongjiang Mohe Observatory of Geophysics, Institute of Geology and Geophysics, Chinese Academy of Sciences, Beijing, China, [3]Institute of Geophysics and Planetary Physics, University of California, Santa Cruz, CA, USA

Key Points:

- A high-resolution broadband crustal attenuation model is obtained for the SE Tibetan Plateau based on high-density ChinArray Lg-wave data
- Frequency-dependent Lg attenuation suggests that brittle and viscous deformation occur in the mid-to-upper and lower crust, respectively
- The crustal flow corridors are partially interconnected but not truncated in the core region of the Emeishan Large Igneous Province

Supporting Information:

Supporting Information may be found in the online version of this article.

Correspondence to:

L.-F. Zhao,
zhaolf@mail.iggcas.ac.cn

Citation:

He, X., Zhao, L.-F., Xie, X.-B., Li, R.-J., Lu, T., & Yao, Z.-X. (2026). Hindered but not halted crustal flow: Implications from Lg-wave attenuation tomography based on high-density ChinArray in SE Tibetan Plateau. *Journal of Geophysical Research: Solid Earth*, *131*, e2025JB032994. https://doi.org/10.1029/2025JB032994

Received 15 SEP 2025
Accepted 5 MAR 2026

Author Contributions:

Conceptualization: Xi He, Lian-Feng Zhao, Xiao-Bi Xie
Data curation: Xi He, Lian-Feng Zhao
Formal analysis: Xi He, Lian-Feng Zhao, Ruo-Jie Li, Tong Lu
Funding acquisition: Xi He, Lian-Feng Zhao, Zhen-Xing Yao
Investigation: Xi He
Methodology: Xi He, Lian-Feng Zhao, Xiao-Bi Xie
Project administration: Lian-Feng Zhao, Zhen-Xing Yao
Software: Xi He, Lian-Feng Zhao, Ruo-Jie Li, Tong Lu
Supervision: Lian-Feng Zhao, Xiao-Bi Xie, Zhen-Xing Yao
Validation: Xi He
Visualization: Xi He, Tong Lu
Writing – original draft: Xi He

© 2026. American Geophysical Union. All Rights Reserved.

Abstract In response to the continuous Indian-Eurasian plate convergence, the mechanically weak crust of the Chuan-Dian block in the SE Tibetan Plateau moves southeastwards, representing one of the significant expanding margins of the Tibetan Plateau. However, whether such crustal movement is impeded by the localized rigid crust associated with the Permian magmatic activities in the Emeishan Large Igneous Province (ELIP) remains controversial. Here, based on the high-density ChinArray Lg data, we invert for a high-resolution broadband attenuation model of the SE Tibetan crust. The Chuan-Dian block is characterized by a low Q_{Lg} below 200 over the frequency range 0.2–2.0 Hz. In contrast, at frequencies above 2.5 Hz, the low Q_{Lg} is concentrated near major strike-slip faults. This is consistent with a lower-crustal flow model underlying the relative movement of upper-crustal blocks. Between the significant low-Q_{Lg} anomalies in the northern and southern Chuan-Dian block, there is an abrupt ~30% increase in Q_{Lg} between 2.5 and 10.0 Hz, reflecting the magma-modified crust in the ELIP core that gained mechanical strength during cooling. The lateral Q_{Lg} variation corresponds to a ~1 order of magnitude increase in strength, which may indicate an obstructive effect. However, the broadband Q_{Lg} images suggest a depth-varying crustal strength, possibly due to the impact of asthenosphere upwelling associated with eastward subduction of the Indian Plate. Combining with S-wave velocity and Pg-wave attenuation, our Lg attenuation suggests that the ELIP core can only partially hinder the crustal flow rather than completely halt it.

Plain Language Summary The topographic trend in the SE Tibetan Plateau resembles a southeastward crustal flow. However, geological records and geophysical observations indicate that the Emeishan Large Igneous Province (ELIP) core, with increased crustal strength, may serve as a conduit for the flow. However, whether such a localized structure would block crustal flow remains debated. In this study, we utilize Lg-wave amplitude data from very dense seismic arrays to map crustal attenuation in the SE Tibetan Plateau. Broadband strong attenuation correlates with a variety of geophysical anomalies in the mid-lower crust and with the distribution of major active faults, consistent with a hybrid crustal flow model that incorporates both viscous and brittle deformation. We identified a patch of weak attenuation that correlates with the ELIP core, whose crustal strength is estimated to exceed 10^{21} Pa · s, exceeding that of the surrounding flowing material. The increase in strength appears to result from cooled, magma-modified mid-upper crust, whereas the mid-lower crust may remain hot and soft due to asthenospheric upwelling. In this scenario, the weak crustal flow around the ELIP core could still be connected at certain depths, allowing the SE Tibetan Plateau to expand beyond such obstruction.

1. Introduction

The formation of the Tibetan Plateau, generally ascribed to the convergence of the Indian and Eurasian plates, could have involved multiple mechanisms, including continental collision, lithospheric delamination, tectonic extrusion, and lower-crustal flow (Ding et al., 2022). During the continental collision, the crust of the Tibetan Plateau could be thickened by both the shortening of plateau terranes, such as the Songpan-Ganzi, Qiangtang, and Lhasa terranes, and the superposition of the underthrusting Indian lithosphere and the overlying Eurasian lithosphere (Yin & Harrison, 2000). Lithospheric delamination suggests that the lithospheric mantle beneath the central Tibetan Plateau may have been removed due to gravitational instability of the thickened lithosphere, and that associated asthenospheric upwelling would further elevate the topography (Owens & Zandt, 1997). Lateral

Writing – review & editing: Xi He, Lian-Feng Zhao, Xiao-Bi Xie, Ruo-Jie Li, Tong Lu

growth of the Tibetan Plateau, in addition to its vertical growth, is also under heated debate. The tectonic extrusion focused on strike-slip motion along major faults, including the Altyn Tagh, Haiyuan, Kunlun, Xianshuihe, and Red River faults, which facilitated the eastward migration of plateau terranes and created expanding frontiers in the eastern Tibetan Plateau (Tapponnier et al., 2001). In contrast, crustal flow was proposed to account for differences in topographic variation between the eastern Tibetan Plateau and its surroundings (Royden et al., 2008). Remarkable lateral growth is evident in the SE Tibetan Plateau, making this region crucial for clarifying the competing mechanisms and enhancing our understanding of the Tibetan Plateau's formation and evolution.

During the lateral growth of the Tibetan Plateau, the SE Tibetan Plateau is regarded as one of the expanding margins of the plateau (Figure 1), as the present-day Global Navigation Satellite System (GNSS) velocity field revealed a flow spreading eastward and around the EHS (Kreemer et al., 2014; Todrani et al., 2022). The expansion of the SE Tibetan Plateau mainly manifests southeast-ward translation and clockwise rotation of the Chuan-Dian block, which produces ∼11.8–14.5 mm/yr and ∼13–15 mm/yr right-lateral strike-slip motions on its northeastern and eastern boundaries, the Xianshuihe fault and Xiaojiang fault, respectively (W. Wang et al., 2021; M. Wang & Shen, 2020). The northeast-striking Lijiang fault crossing the Chuan-Dian block accommodates the movement of the block through the ∼4.3 mm/yr left-lateral strike-slip, resulting in two sub-blocks: the West-Sichuan in the north and the Central-Yunnan in the south (W. Wang et al., 2021). The related deformation concentrates near the boundaries of geological blocks and could be explained by the extrusion of crustal blocks. On the contrary, in the mid-lower crust, geophysical observations, including low seismic wave speeds, high conductivity, and strong seismic attenuation, indicate the presence of partial melting and weak materials (e.g., Bai et al., 2010; Bao et al., 2015; L. F. Zhao, Xie, He, et al., 2013). The pattern of these anomalies shows a south- and southeastward trend across geological boundaries, generally following the direction of surface movement, and therefore supports the mid-lower crustal flow model in building the topography of the SE Tibetan Plateau (e.g., Y. Li et al., 2019). To reconcile the two tectonic models, a hybrid model has been proposed in recent years that incorporates both the brittle shallow crust and the ductile deep crust (Q. Y. Liu et al., 2014). Under this assumption, the flow of the viscous lower crust, driven by gravity and tectonic stress, may drag the overlying brittle upper crustal blocks, resulting in strike-slip motion and seismicity along faults between geological blocks. However, some studies suggest that the isolation of low-velocity anomalies indicates disconnection within the assumed crustal flow (X. Yang, et al., 2023; Z. Zhang et al., 2020). The separation occurred in the Central Yunnan block, which corresponds to the core of the ELIP, where the Late Permian basaltic flood may have altered the crustal composition through magma underplating and intraplate magmatism. Whether these variations in strength could divert or even impede the outflow of plateau crustal materials remains controversial (Han et al., 2022; Qiao et al., 2018).

Seismic attenuation provides insights into the dynamics of seismic wave propagation and the underlying mechanical properties, along with seismic velocity, which is associated with propagation kinematics (Aki & Richards, 2002). It describes the phenomenon in which seismic waves decay, in addition to geometrical spreading, as they travel through a medium with heterogeneities arising from structures and anomalies in physical properties, including temperature, strength, and fluid content (Boyd et al., 2004). It is usually quantified by the quality factor (Q), defined as the reciprocal of the fractional loss of seismic energy per cycle (Shearer, 2009). Since Q values often range from hundreds to thousands, whereas within the crustal velocity perturbations are typically on the order of 10%, Q can be considered a sensitive and effective tool for demonstrating crustal characteristics. In the SE Tibetan Plateau, seismic Q models for P and S waves have been obtained based on local earthquake data tomography or full-waveform inversions, revealing a relationship between the seismic attenuation and regional tectonics, such as mid-lower crustal flow, deep melting, and seismogenic structures (Dai et al., 2020; Duan et al., 2024; Tang et al., 2022). Through decades of development, seismic attenuation tomography provides an alternative approach to constructing a large-scale, high-resolution, and broadband Q_{Lg} model, primarily due to the efficient propagation of Lg waves within the continental crust, which yields a readily available and considerable amount of Lg amplitude data (e.g., Ma et al., 2023; Shen et al., 2023; L. Zhang et al., 2022). Because the Lg wave represents high-frequency S-wave energy trapped within the crust, consisting of high-mode surface waves and crustal reverberation of converted P and SV waves, the Q_{Lg} generally reflects the attenuation response of the whole crust and could be assumed as a proxy of average crustal attenuation of S waves. Early work on eastern Eurasia reported a significantly stronger Lg attenuation in the Tibetan Plateau and its surroundings (Xie et al., 2006). Q_{Lg} images with high resolution of ∼1–2° but limited coverage over the SE

21699356, 2026, 3, Downloaded from https://agupubs.onlinelibrary.wiley.com/doi/10.1029/2025JB032994 by Institution Of Geology, Wiley Online Library on [19/04/2026]. See the Terms and Conditions (https://onlinelibrary.wiley.com/terms-and-conditions) on Wiley Online Library for rules of use; OA articles are governed by the applicable Creative Commons License

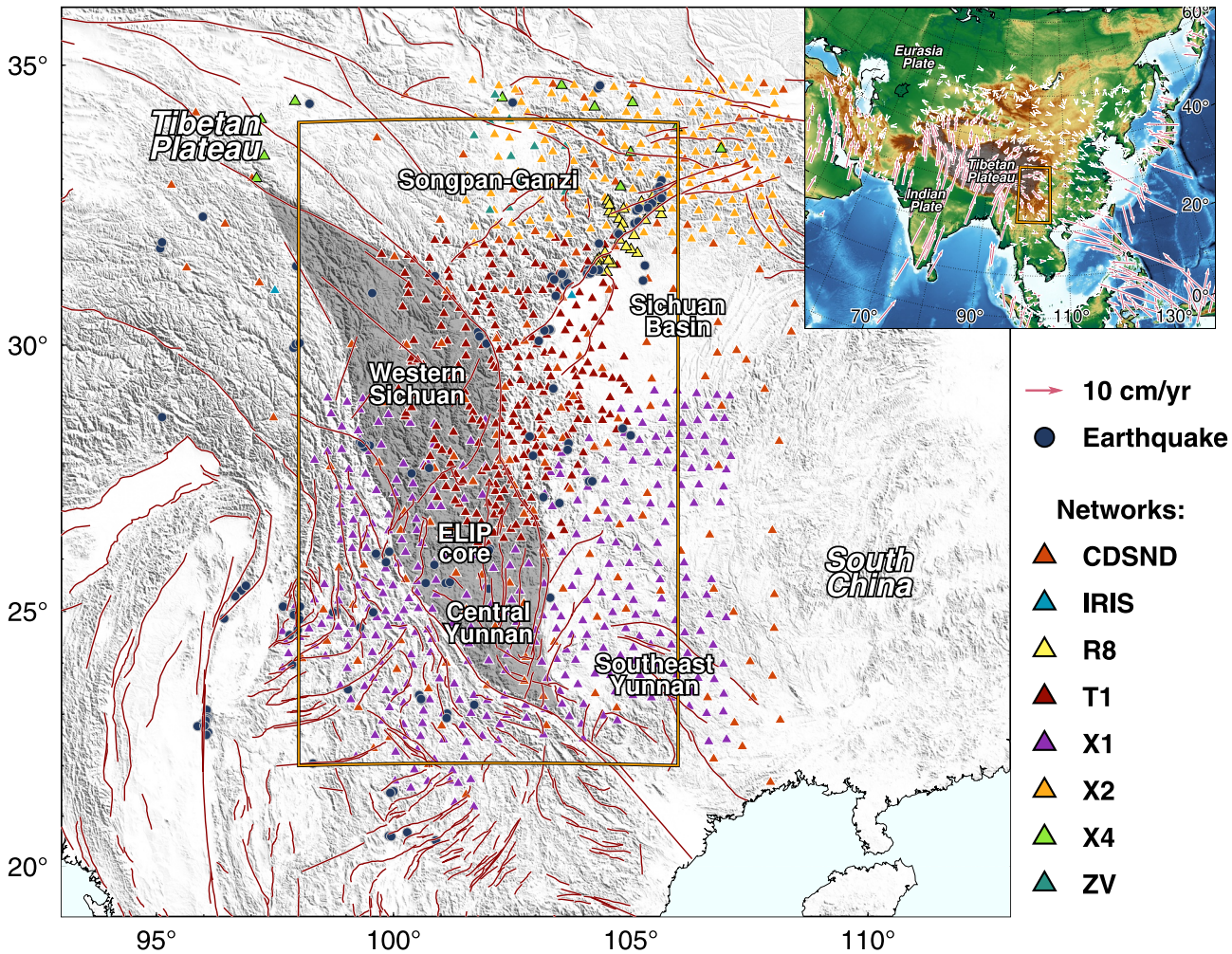

Figure 1. Map showing the topography of the SE Tibetan Plateau and distributions of the seismic stations and the earthquakes used in this study. The insert map shows the location of the study region in a larger-scale map, overlain by Global Navigation Satellite System velocities (red arrows; Kreemer et al., 2014). The black-shaded area denotes the Chuan-Dian block, comprising the West Sichuan and Central Yunnan blocks, with the Emeishan Large Igneous Province core located between them.

Tibetan Plateau were also obtained (Bao et al., 2011; Y. Chen & Xie, 2017). Bao et al. (2012) suggested that shear-strain heating along major strike-slip faults led to a hot crust, thereby resulting in strong attenuation of Lg waves. L. Q. Zhou et al. (2008) attributed the high-attenuation anomalies in their Q_{Lg} model to fractured materials and hot migration within fault zones, while the low attenuation was attributed to mild crustal deformation, seismicity, and hydrothermal activity in stable terranes. By incorporating multiple geophysical, geological, and geodetic observations, L. F. Zhao, Xie, He, et al. (2013) constrained lower-crustal flow at a larger scale based on the distribution of low Q_{Lg}, which stretched from the northern to the eastern Tibetan Plateau and then turned southeastward along the western edge of the rigid Sichuan Basin. He et al. (2021) further tracked this elongated low-Q_{Lg} anomaly in the SE Tibetan Plateau. They suggested relatively weak, complex connectivity for the flow of crustal material, possibly because the ELIP partly blocked, but did not entirely truncate, the flow. However, due to limited data coverage or image resolution in previous studies, the fine-scale distributions of strong and weak Lg attenuation remain to be further investigated to constrain the local mechanisms that contribute to crustal deformation in the SE Tibetan Plateau.

In this study, we collect Lg amplitude data from densely spaced seismic stations to refine the tomographic Q_{Lg} model for the SE Tibetan Plateau. The relationships between the Q_{Lg} and crustal rheology, as well as other geophysical, geological, and geodetic observations, will be discussed, so that we can explore the origins of anomalous Lg attenuation, the distributions of flow of crustal materials, the interplay between the flow and local tectonic structures, and finally improve our understanding of the expansion of the Tibetan Plateau.

21699356, 2026, 3, Downloaded from https://agupubs.onlinelibrary.wiley.com/doi/10.1029/2025JB032994 by Institution Of Geology, Wiley Online Library on [19/04/2026]. See the Terms and Conditions (https://onlinelibrary.wiley.com/terms-and-conditions) on Wiley Online Library for rules of use; OA articles are governed by the applicable Creative Commons License

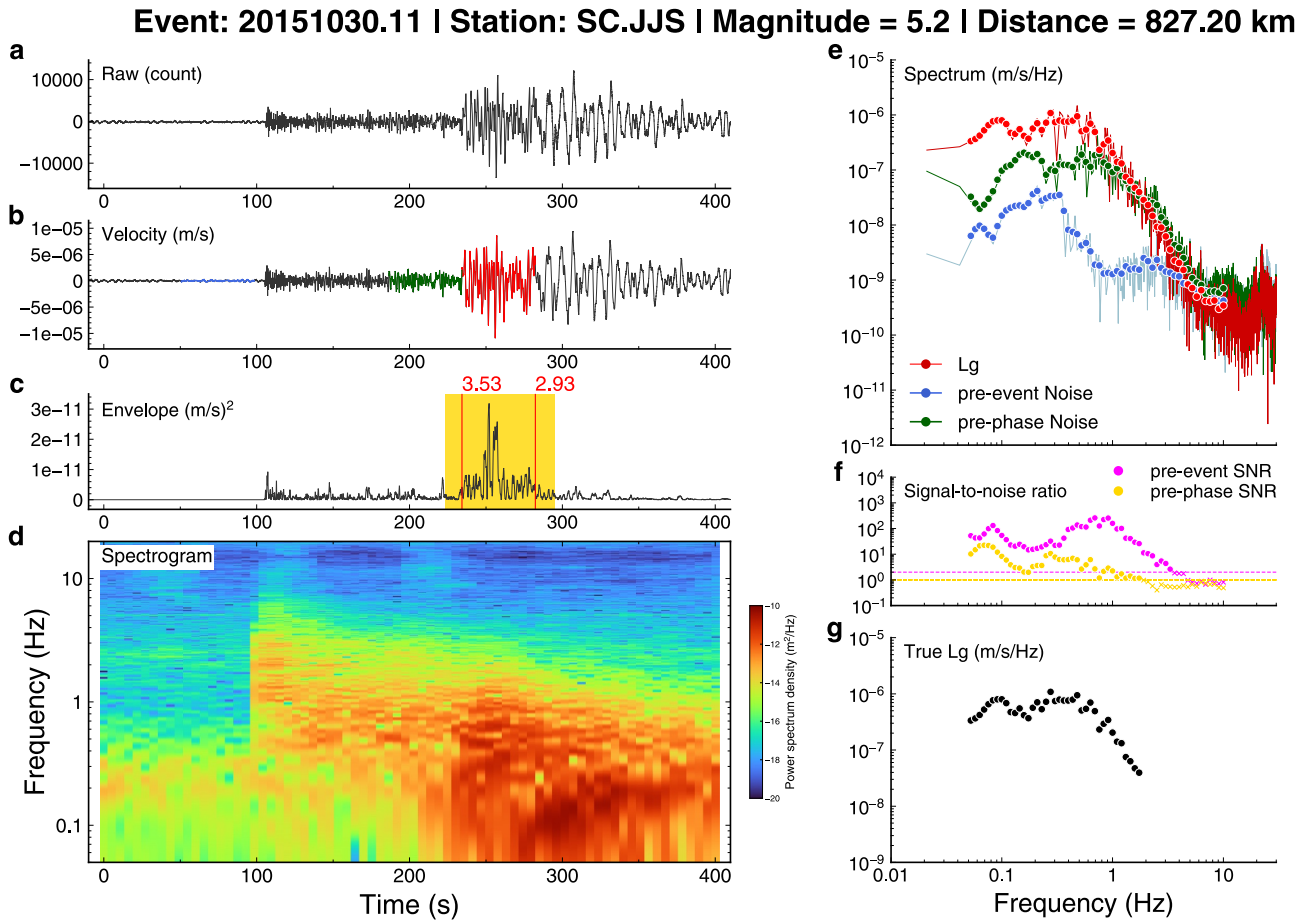

Figure 2. Preprocessing of the Lg waveform. Event and station information is labeled at the top. (a) Raw data. (b) Velocity waveform after removing the instrumental response. Lg, pre-event noise, and pre-phase noise are plotted in red, blue, and green. (c) Energy envelope between 0.5 and 1.5 Hz. A sliding velocity window with a length of 0.6 km/s moves within the range of 3.7–2.8 km/s (yellow interval), within which the average energy is calculated. The Lg window is determined based on the maximum energy (vertical red lines). (d) Time-frequency spectrogram obtained using the short-time Fourier transform. Remarkable Lg energy is visible within the Lg window over a broad frequency range. (e) Spectra of the Lg, pre-event noise, and pre-phase noise. (f) Pre-event and pre-phase signal-to-noise ratios. (g) The resulting Lg spectra after correcting for the pre-event noise.

2. Data and Methods

We selected 134 earthquakes between 2007 and 2016 in the SE Tibetan Plateau from the International Seismological Center earthquake catalog, with their focal depths shallower than local CRUST 1.0 Moho depths to ensure crustal events, and their magnitudes between 4.4 and 6.4 to avoid Lg being dwarfed by noise and contamination from complex focal rupture processes of large earthquakes (Table S1 in Supporting Information S1). We then collected a total of 39,967 vertical-component seismograms recorded at 1,038 permanent and temporary seismic stations from the China Digital Seismic Array, the ChinArray Program (X. F. Zheng et al., 2010), and the Incorporated Research Institutions for Seismology (Figure 1 and Table S2 in Supporting Information S1).

The Lg-wave can be recognized by its prominent amplitudes, vague onset, and relatively long wavetrain (Figure S1 in Supporting Information S1). We first obtained the Lg spectral amplitudes and amplitude ratios between 0.05 and 10.0 Hz (Text S1 in Supporting Information S1), following a previous Lg amplitude pre-processing procedure (L. F. Zhao, Xie, Wang, et al., 2013). To ensure reliable Lg measurements, adaptive Lg windows were used for each seismogram to capture the maximum Lg energy, and the amplitudes were screened to exceed 1 times the pre-phase noise and 2 times the pre-event noise. The noise was corrected by calculating the square root of the difference between the squares of Lg and pre-event noise (Figure 2). No significant focusing/defocusing effects were observed in the data (Figure S2 in Supporting Information S1), possibly due to the higher dominant frequency and

21699356, 2026, 3, Downloaded from https://agupubs.onlinelibrary.wiley.com/doi/10.1029/2025JB032994 by Institution Of Geology, Wiley Online Library on [19/04/2026]. See the Terms and Conditions (https://onlinelibrary.wiley.com/terms-and-conditions) on Wiley Online Library for rules of use; OA articles are governed by the applicable Creative Commons License

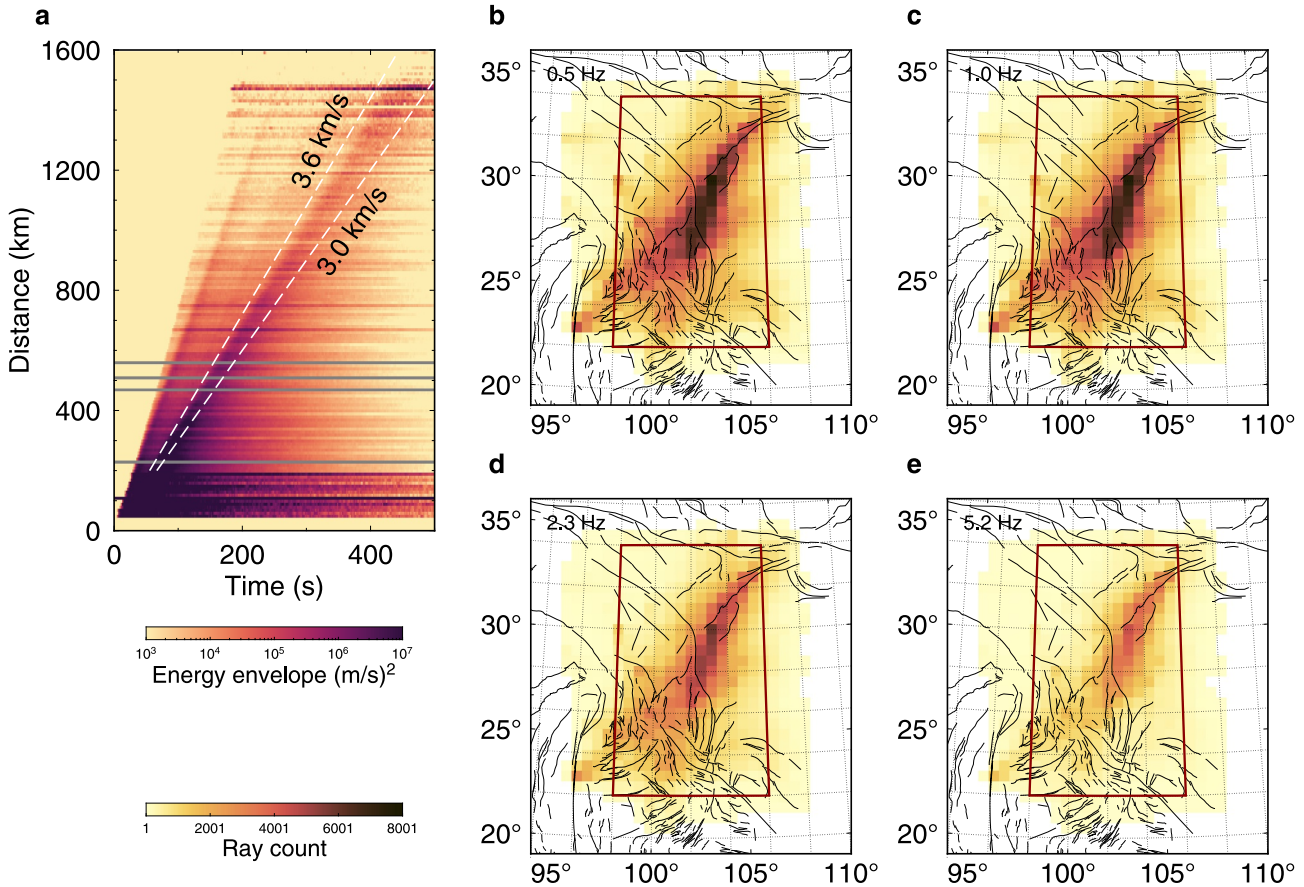

Figure 3. (a) Energy envelop plot showing the development of major regional seismic phases. Lg-wave is highlighted by the velocity window of 3.6–3.0 km/s (dashed lines). The energy is stacked from envelopes in the vertical component between 0.5 and 1.5 Hz over the epicentral bins of 4 km. (b–e) The maps of raypath count per tomographic grid for 0.5, 1.0, 2.3, and 5.2 Hz.

the highly reverberant nature of Lg-wave. From the focal distance profile of the stacked energy envelopes of all the seismograms (Figure 3a), the Lg wave is well-developed over a propagation range of more than ~1,400 km. The well-developed Lg ensures the intensive ray-path coverage (Figures 3b–3e). The ratio of Lg amplitudes can be calculated further when an earthquake is recorded at two stations roughly aligned. The two-station Lg amplitude data have minimized source effects. Then, Lg attenuation tomography was conducted using an established method that included linearization of Lg amplitude synthesis and the use of the least-squares QR factorization to iteratively solve for both the attenuation and the source term of the Lg waves (Paige & Saunders, 1982; L. F. Zhao, Xie, Wang, et al., 2013).

3. Results

The Lg attenuation for the SE Tibetan Plateau is obtained independently at 58 frequencies between 0.05 and 10.0 Hz, with lateral resolution reaching 0.5° (Figure S3 in Supporting Information S1), and the relative error in Q_{Lg} values mostly being below 20% (Figure S4 in Supporting Information S1). To strengthen the Lg modeling, we invert for the site term after obtaining attenuation and source terms (Text S3 and Figure S5 in Supporting Information S1). Our tomographic Q_{Lg} model exhibits notable lateral variations corresponding to terranes, with improved details on the distribution of Q_{Lg} anomalies compared with a previous study using similar Lg processing and attenuation imaging methods (He et al., 2021) (Figure S6 in Supporting Information S1). Weak Lg attenuation is observed in the South China block, which includes the Sichuan Basin and Southeastern Yunnan. In contrast, the Tibetan Plateau and its southeastern margin exhibit pronounced Lg attenuation, indicating substantial absorption of seismic energy. At 1.0 Hz, the low Q_{Lg} anomalies of below 200 in the Songpan-Ganzi block are confined by the LMSF in the southeast and stretch southward across the XSHF and into the Chuan-Dian block

21699356, 2026, 3, Downloaded from https://agupubs.onlinelibrary.wiley.com/doi/10.1029/2025JB032994 by Institution Of Geology, Wiley Online Library on [19/04/2026]. See the Terms and Conditions (https://onlinelibrary.wiley.com/terms-and-conditions) on Wiley Online Library for rules of use; OA articles are governed by the applicable Creative Commons License

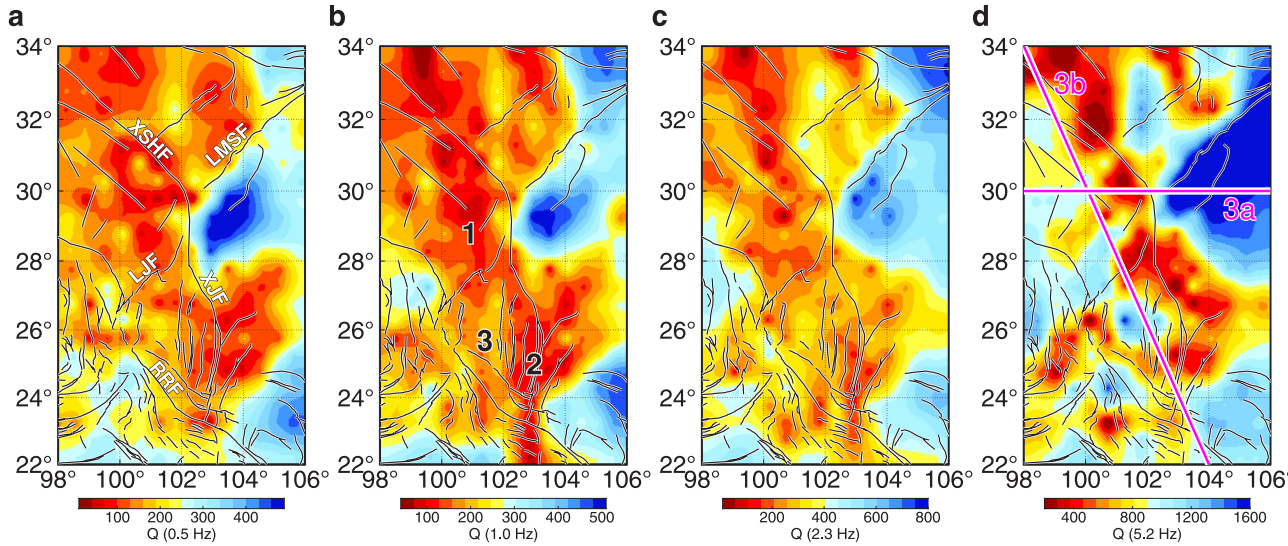

Figure 4. Q_{Lg} maps at 0.5 (a), 1.0 (b), 2.3 (c), and 5.2 Hz (d). Fault traces are shown by thin black lines, with abbreviations of major faults labeled (LMSF: Longmenshan fault; XSHF: Xianshuihe fault; XJF: Xiaojiang fault; LJF: Lijiang fault; RRF: Red River fault). Magenta lines in (d) represent the locations of profiles in Figure 5.

(Figure 4b). Both sub-blocks of the Chuan-Dian block, the Western Sichuan and Central Yunnan, exhibit significant strong Lg attenuation, characterized by pervasive low Q_{Lg} below 200 and 100 (denoted as Anomalies #1 and #2 in Figure 4b). Note that a localized anomaly of Q_{Lg} around 250 emerges between the low-Q_{Lg} #1 and #2, corresponding to the core area of the ELIP (denoted as anomaly #3 in Figure 4b). Such pattern around the Chuan-Dian block can be seen on Q_{Lg} maps across frequencies despite of the increase in Q_{Lg} with frequency, and is more pronounced for higher frequencies. For example, at 5.2 Hz, the elevated Q_{Lg} in the ELIP core exceeds 1000, which is higher than the ~400–800 Q_{Lg} values in the surrounding areas of the Chuan-Dian block. At the 5.2 Hz Q_{Lg} map, low Q_{Lg} values tend to be concentrated near the major strike-slip XSHF and XJF faults that accommodate the tectonic movement of the Chuan-Dian block, suggesting contributions to Lg decay from scattering due to shear deformation near the fault system.

4. Discussions

4.1. Weak Crust in the SE Tibetan Plateau

The correspondence of Q_{Lg} to terranes suggests a close relationship between Lg attenuation and regional tectonics. The Sichuan Basin is characterized by relatively weak Lg attenuation, which can be explained by a rigid, cooled cratonic lithosphere with minimal intracratonic deformation and faulting (S. Liu, et al., 2021). These attributes favor the efficient propagation of seismic waves. In Southeastern Yunnan, high Q_{Lg} values may be associated with the ancient Laojunshan gneiss dome structure. Geological and geochemical investigations indicate that this structure was formed by magma intrusion during the Paleozoic and underwent significant uplift and exhumation during the Mesozoic and Cenozoic periods (Z. Liu, et al., 2021). Weak Lg attenuation in this region may be related to the ancient rocks and reduced fluid content resulting from metamorphism. The strong Lg in the SE Tibetan Plateau could indicate active tectonics. Consistent with previous Lg attenuation studies (Bao et al., 2012; He et al., 2021; Wei & Zhao, 2019), our tomographic model reveals remarkable lateral variations in Lg attenuation with improved resolution. Similar patterns of seismic attenuation were also observed based on various methodologies. Full waveform tomography reveals strong attenuation in the upper mantle for the northern Chuan-Dian, reflecting its connection to the "crustal flow" in this region (Tang et al., 2022). Rayleigh waves propagate efficiently with low attenuation within the Sichuan Basin, but are highly attenuated in the Western Sichuan block (J. Chen et al., 2012; L. Zhou et al., 2020). Observation of teleseismic P waves suggested that both the weak attenuation beneath the Sichuan Basin and the strong attenuation beneath the eastern Tibetan Plateau could extend to depths of 200 km. In contrast, the Central Yunnan region is featured by depth-dependent attenuation (H. Liu et al., 2024). Attenuation tomography at local scales could reveal finer structures at

21699356, 2026, 3, Downloaded from https://agupubs.onlinelibrary.wiley.com/doi/10.1029/2025JB032994 by Institution Of Geology, Wiley Online Library on [19/04/2026]. See the Terms and Conditions (https://onlinelibrary.wiley.com/terms-and-conditions) on Wiley Online Library for rules of use; OA articles are governed by the applicable Creative Commons License

21699356, 2026, 3, Downloaded from https://agupubs.onlinelibrary.wiley.com/doi/10.1029/2025JB032994 by Institution Of Geology, Wiley Online Library on [19/04/2026]. See the Terms and Conditions (https://onlinelibrary.wiley.com/terms-and-conditions) on Wiley Online Library for rules of use; OA articles are governed by the applicable Creative Commons License

shallow depths. Duan et al. (2024) attributed the high-attenuation corresponding to our anomaly #2 to deep melting, and Dai et al. (2020) suggested that the low-attenuation for the ELIP core could divert the crustal flow.

Our broadband strong Lg attenuation aligns with a variety of geophysical observations, suggesting possible depth-varying tectonic origins, including variations in fluid content, temperature, and partial melting in the middle-lower crust, as well as fault development in the upper-middle crust. The low Q_{Lg} between 0.2 and 2.0 Hz of Anomaly #1 in the Songpan-Ganzi and northern Chuan-Dian correlates well with significant anomalies of low S-wave velocity in the mid-lower crust (e.g., Bao et al., 2020; C. Zheng et al., 2019). For example, based on joint inversion of Rayleigh wave and teleseismic body wave, X. Yang, et al. (2023) revealed anomalies of low S wave velocity for this region at depths between 20 and 40 km, with the absolute velocity value less than 3.3 km/s. Previous studies have suggested that a velocity of 3.5 km/s in the mid-lower crust is an indicator of partial melting (e.g., Y. J. Yang et al., 2012). Strong attenuation for Anomaly #1 is also linked to the observed broad zone of high crustal conductivity near LJF at depths ranging from ∼25 to 50 km, which required a melt fraction of ∼5%–15% to account for (X. Li et al., 2020). Experimental observations indicate that such a melt fraction (∼5%–15%) would reduce viscosity by a factor of ∼6–200 (Yamauchi & Takei, 2024). Therefore, Anomaly #1 could suggest a remarkably weak mid-lower crust.

Another prominent low-Q_{Lg} anomaly, Anomaly #2, is revealed in Central Yunnan near the XJF, characterized by low Q_{Lg} values below 150 in the 0.2–2 Hz frequency range, which also corresponds to low S-wave velocity (Y. Y. V. Fu et al., 2017) and high conductivity (Cui & Chen, 2023). For example, S. Zhao et al. (2024) revealed a significantly low-velocity anomaly near the XJF at depths of 25–30 km based on ambient noise interferometry waveforms. They attributed the anomaly to the felsic lower midcrust, which is characterized by lower melting temperatures and weaker strength. Their findings on crustal composition were consistent with a low Poisson's ratio of ∼0.2–0.25 in this area (W. L. Wang et al., 2017). Therefore, Anomaly #2, strong Lg attenuation could be attributed to partial melting in the mid-lower crust, which absorbs seismic energy through viscous deformation.

Under the crustal flow model, the weakened, viscous mid-lower crust would flow in response to gravity and lateral tectonic stress (e.g., Royden et al., 2008). The gravity data suggest a non-isostatic state of the SE Tibetan Plateau, which may be attributed to horizontal forces from adjacent crust (B. Liu et al., 2017). By fitting the observed GPS velocities, finite-element simulations suggest that gravitational spreading shapes the crustal deformation of the SE Tibetan Plateau, with lateral tectonic driving forces contributing to a better fit (Y. Li et al., 2019). Therefore, the weak mid-lower crust revealed by the strong Lg attenuation Anomalies #1 and #2 between 0.2 and 2.0 Hz could indicate a flow beneath Western Sichuan and Central Yunnan. Radial anisotropy, described by the velocities of SH- and SV-waves, revealed a horizontal preferred orientation of anisotropic materials (Y. V. Fu et al., 2018; H. Huang et al., 2010), which can be linked to horizontal viscous flow in this area.

As frequency increases to ∼3 Hz and above, low-Q_{Lg} Anomalies #1 and #2 develop more concentrated around the XSHF and the XJF (Figure 4d), which may reflect the role of major strike-slip faults in addition to the viscous flow in the mid-lower crust. The two active faults accommodated the motions of the Western Sichuan and Central Yunnan blocks (W. Wang et al., 2021). Scattering effects from porosity and cracks within fault zones can reduce seismic wave amplitudes, thereby lowering Q_{Lg} at higher frequencies. In addition, significant shear strain exceeding 6×10^{-8}/yr was observed for these faults (Y. Li et al., 2019), and the associated shear heating effect could indicate further seismic energy dissipation (Bao et al., 2012). Therefore, the strong Lg attenuation at higher frequencies might suggest mechanically weak zones at shallow depths for the XSHF and XJF, where brittle deformation related to fault activities can facilitate the southeastward movement of upper-crustal blocks of the Wester Sichuan and Central Yunnan. Combining the Lg attenuation features for both ∼0.2–2 Hz and ∼3–5 Hz, our Q_{Lg} model suggests a flow of weak crustal materials, which includes both viscous flow within the mid-lower crust and brittle deformation for the upper crust. In this case, coupling between deep and shallow parts of the crust is expected, which could be manifested as consistencies between the upper-crustal and whole-crustal anisotropies for XSHF and XJF (Y. Li & Gao, 2023).

4.2. Potential Impedance From Emeishan Large Igneous Core

On the frequency cross-section along a profile traversing the Western Sichuan and Sichuan Basin (Figure 5a), abrupt lateral variation in Q_{Lg} over a broad frequency band was revealed across the XSHF and LMSF. At frequencies below ∼0.2 Hz, the Sichuan Basin exhibits greater attenuation than Western Sichuan, which may be attributed to scattering within the thick sediments (e.g., Guo et al., 2022). Although Lg is considered a guided

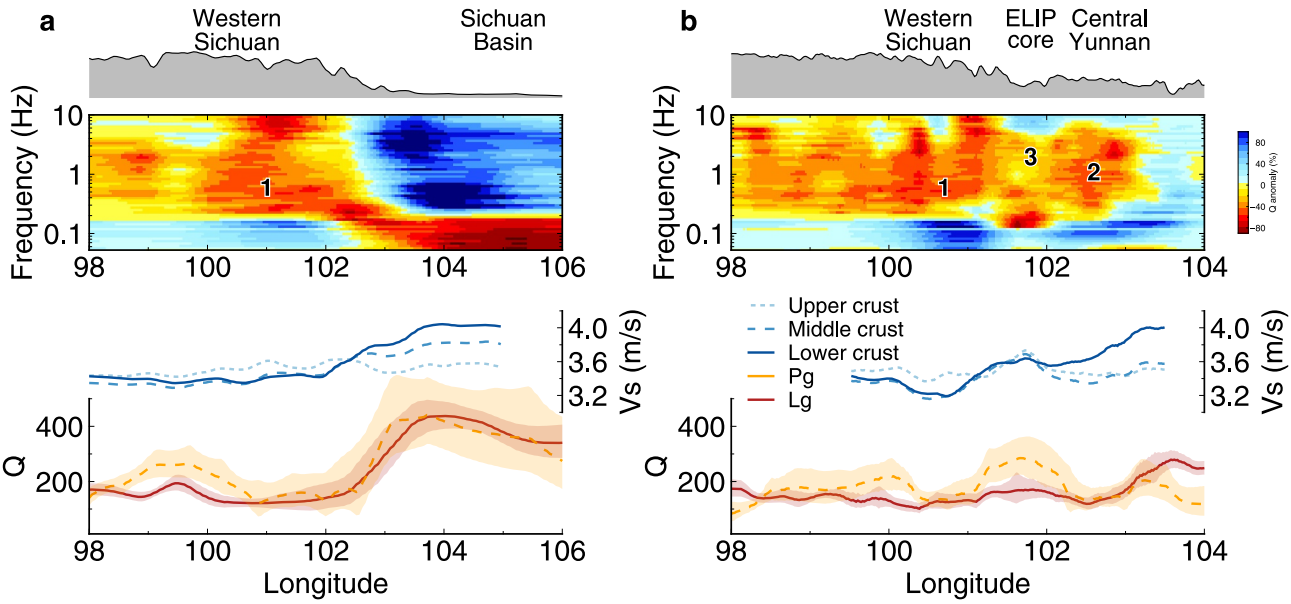

Figure 5. The frequency cross-sections. The locations of the profiles are shown in Figure 4d. In each panel, the topographic elevation, Q_{Lg} versus frequency, comparison of average 0.3–2.0 Hz Q_{Lg}, crustal S-wave velocity (Y. Liu, et al., 2021), and 0.2–2.0 Hz average Pg-wave Q (R. J. Li et al., 2023) are shown from top to bottom. The S-wave velocity is calculated for depth ranges of 10–20, 20–30, and 30–40 km, representing the upper, middle, and lower crust, respectively.

wave within the crust, the reverberation trapped in the thick sediments could dominate Lg attenuation at lower frequencies. Assuming that scattering effects dominate, the strong Lg-wave attenuation anomaly can be related to the wavenumber k and the dominant scale of the scatterers a via ka = 1 (Wu et al., 2000). Thus, the absorbing band at 0.05–0.2 Hz could indicate scattering scales of approximately 3–11 km, corresponding to the ~10 km-thick sediment layer in the Sichuan Basin. A similar but less pronounced phenomenon is observed for the ELIP core, where strong Lg attenuation occurs between ~0.1 and 0.2 Hz, indicating scattering scales of ~2–10 km. This is consistent with the Mesozoic sediment thickness within this region (e.g., Shi et al., 2023). In contrast, at frequencies above ~0.2 Hz, Western Sichuan exhibits Q_{Lg} values that are significantly lower than those in the Sichuan Basin. This observation corresponds to pronounced local changes in S-velocity within the mid-lower crust (Y. Liu et al., 2023) and in Pg attenuation (R. J. Li et al., 2023), suggesting a mechanical strength contrast between Western Sichuan and the Sichuan Basin that would block mid-lower-crustal flow in the east. The impending effect is consistent with the topographic change along this profile. Based on the southeastward decreasing trend in regional topography and the GNSS velocity field in southeast-south direction (e.g., G. Zheng et al., 2017), the crustal flow for Anomaly #1 in the Western Sichuan could be diverted south toward Anomaly #2 in the Central Yunnan. On the profile, generally along the assumed crustal flow (Figure 5b), significantly low Q_{Lg} values persist across a broad frequency band for Anomalies #1 and #2. However, patches of normal-to-high Q_{Lg} at various frequencies are revealed beneath the ELIP core area (Anomaly #3), characterized by normal Q_{Lg} values between ~0.5 and 2 Hz, and more pronouncedly, a 40% increase in Q_{Lg} above 3 Hz, among anomalies of extreme attenuation. The correspondence to high Q_{Pg} and high S-wave velocity indicated an elevated average strength of the whole crust of the ELIP core, which may obstruct the crustal flow sourced from Anomaly #1. By interpreting the 3D S-wave velocity and anisotropy model inverted from Rayleigh waves, Han et al. (2022) revealed a strengthened structure beneath the ELIP core at depths shallower than approximately 20 km, characterized by high velocity and weak anisotropy. They also found that the anisotropy in the area between Western Sichuan and Central Yunnan was oriented NE-SW, generally parallel to the boundary, and attributed this feature to pure shear deformation resulting from the rigid ELIP core obstructing the extrusion of crustal materials.

Despite the obstructing effect, the crustal strength of the ELIP core remained unconstrained. Since anelastic deformation and seismic attenuation are both defect-controlled processes, they are expected to vary similarly with depth due to their temperature- and pressure-dependent behavior (Anderson, 1966). The viscosity η can be expressed as $\eta \propto \exp\left(\frac{H_\eta^*}{RT}\right)$, and similarly, the seismic attenuation as $Q^{-1} \propto \exp\left(-\frac{\alpha H_Q^*}{RT}\right)$, where H_η^* and H_Q^* are the activation enthalpy for viscosity and attenuation, respectively, T is temperature, and R is the gas constant

21699356, 2026, 3, Downloaded from https://agupubs.onlinelibrary.wiley.com/doi/10.1029/2025JB032994 by Institution Of Geology, Wiley Online Library on [19/04/2026]. See the Terms and Conditions (https://onlinelibrary.wiley.com/terms-and-conditions) on Wiley Online Library for rules of use; OA articles are governed by the applicable Creative Commons License

21699356, 2026, 3, Downloaded from https://agupubs.onlinelibrary.wiley.com/doi/10.1029/2025JB032994 by Institution Of Geology, Wiley Online Library on [19/04/2026]. See the Terms and Conditions (https://onlinelibrary.wiley.com/terms-and-conditions) on Wiley Online Library for rules of use; OA articles are governed by the applicable Creative Commons License

(Karato, 2010). Assuming viscosity and attenuation are both dependent on temperature, we can have the quantitative relationship between viscosity and attenuation, $\frac{\eta_1}{\eta_2} = \left(\frac{Q_2}{Q_1}\right)^{\frac{1}{\alpha\xi}}$, with $\xi = \frac{H_Q^*}{H_\eta^*}$ (Karato, 2010). This formula shows that the lateral variation in natural logarithmic viscosity is proportional to the lateral variation in natural logarithmic Q, and defines a linear function,

$$\ln \eta = \frac{1}{\alpha\xi}\ln Q - \frac{1}{\alpha\xi}\ln Q_0 + \ln \eta_0, \quad (1)$$

where we can estimate the viscosity based on the Q, given the Q_0 and η_0 for a reference region. The value of $\alpha\xi$ can be obtained from two areas with known Q_{Lg} and η. Previous geodynamic simulations study suggested the viscosity of $\sim 10^{23-24}\mathrm{Pa}\cdot\mathrm{s}$ for rigid Sichuan Basin and $\sim 10^{19-21}\mathrm{Pa}\cdot\mathrm{s}$ for weak mid-lower crust (Pang et al., 2023; J. Yang et al., 2020). Accordingly, we assigned the viscosity of 10^{24} and 10^{21} $\mathrm{Pa}\cdot\mathrm{s}$ to account for the whole crust average viscosity for the Sichuan Basin and Chuan-Dian Block. Based on these values, we can establish a linear relationship between viscosity and attenuation for the SE Tibetan Plateau. The Q_{Lg} results in this study contain both intrinsic and scattering attenuation; however, scattering is not associated with temperature. The terrane-wise statistics indicate that the Q_{Lg} values for the ELIP core generally fell between those of the Chuan-Dian Block and the Sichuan Basin, particularly in the ~0.2–6.0 Hz frequency range. By assuming the power-law model, $Q_{\mathrm{Lg}} = Q_0 f^n$, where f is the frequency, and Q_0 is the 1 Hz Q_{Lg}, the frequency-dependency parameter of Q_{Lg}, n, is also calculated for each geoblock over the frequency range of 0.2–0.6 Hz. Within this range, the Q_{Lg} values show a generally consistent Q_{Lg}-frequency relationship and are less dependent on frequency across the three terranes (Figure 6a), suggesting an absorption-dominant, thermally associated attenuation mechanism. Therefore, to robustly estimate the crustal average viscosity, η was calculated through all Q_{Lg} values between 0.2 and 6 Hz. As shown in Figure 6b, the thin gray lines were linear functions defined by the assigned viscosity and observed Q for the Sichuan Basin and the Chuan-Dian Block. Each line represented one frequency, and the viscosity for the ELIP core was obtained by interpolation using the observed Q_{Lg} at this frequency. Based on the broad band Q_{Lg}, the viscosity was estimated to be 6.38×10^{21} $\left(3.60 \times 10^{21} - 1.13 \times 10^{22}\right)$ $\mathrm{Pa}\cdot\mathrm{s}$. This value remained nearly constant across frequency band choices. Previous study suggested that crustal deformation in the SE Tibetan Plateau included brittle shear zones with strong upper crust and weak lower crust, with the viscosity of larger than 10^{22} and approximately 10^{20} $\mathrm{Pa}\cdot\mathrm{s}$, respectively (J. Yang et al., 2020), which is compatible with our estimate of $\sim 10^{21}$ for the whole crust. Although it varied with the assigned viscosity values, the ELIP core was 6 times (up to 1 order of magnitude) stiffer than the Chuan-Dian Block. Such a strength contrast might lead to the ELIP core obstructing the crustal flow. This is consistent with the localized depressed crust-mantle discontinuity beneath the northern boundary of the ELIP core observed from receiver functions (Xu et al., 2020). Such an obstructing effect would also lead to the distorted morphology of LMSF and LJF (Gan et al., 2021). Observing that the high-velocity ELIP core separated the low-velocity anomalies beneath Western Sichuan and Central Yunnan, Qiao et al. (2018) suggested the crustal flow was diverted around the ELIP core.

However, moderate topographic variation of ~1,000 m across LJF might indicate a limited impeding effect of the ELIP core. In comparison, there is topographic relief over 2,000 m across LMSF, where the variation in Q_{Lg} exceeds 100%, and the contrast in viscosity is assumed to be of three orders of magnitude. One key to understanding whether crustal flow is obstructed is to constrain the distributions and connectivity of the low-velocity and high-attenuation anomalies across depth and frequency. In this study, we evaluated the resolving capability of the tomographic Lg attenuation model for the connectivity between Anomalies #1 and #2. Based on the major observed Q_{Lg} patterns, two models were established with the low-Q_{Lg} anomalies of Western Sichuan and Central Yunnan connected and disconnected, respectively. From the input Q_{Lg} models, spectral amplitudes were synthesized using the obtained source terms and the actual event and station layouts; then, 5% Gaussian noise was added. We inverted for the recovery Q_{Lg} models from the synthesized amplitudes. By comparing the recovery and input Q_{Lg} models, we believe our tomography can detect the ELIP core and the connectivity between Anomalies #1 and #2 (Figure S7 in Supporting Information S1). Therefore, based on Q_{Lg} maps at various frequencies, frequency cross-section profiles, and frequency dependence of Q_{Lg}, a crustal pattern more complex than connected, diverted, or obstructed is suggested.

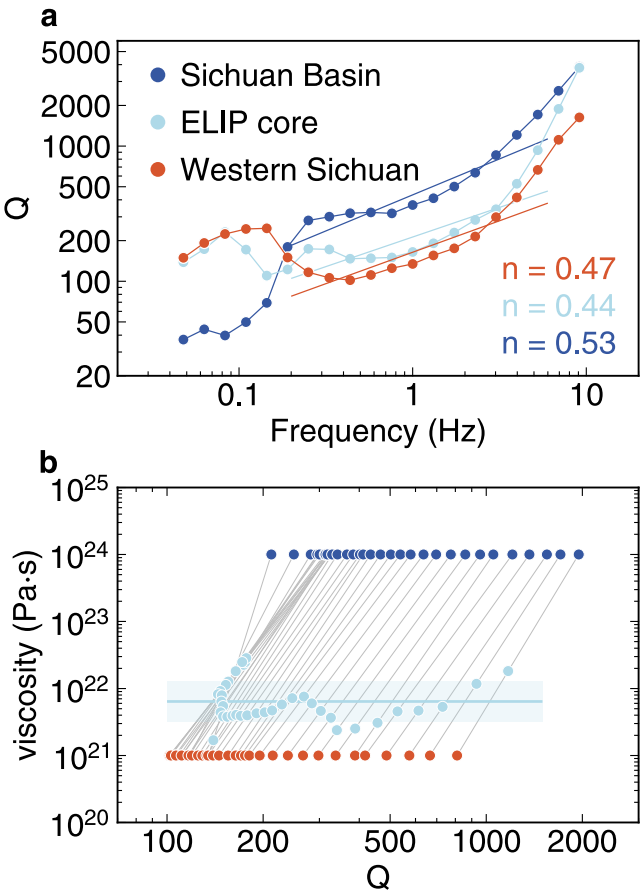

Figure 6. (a) Frequency-dependence of Lg-wave Q. The frequency-dependency of Q_{Lg} is represented by a colored straight line for each geoblock, and the parameter n is labeled at the bottom right. (b) Viscosity estimation. The color scheme for the Sichuan Basin, Emeishan Large Igneous Province (ELIP) core, and Chuan-Dian Block is consistent with that shown in panel (a). The Circle represents Q_{Lg} values obtained between 0.2 and 6 Hz. For Sichuan Basin and Chuan-Dian Block, the values of viscosity are set to 10^{24} and 10^{21} Pa · s, respectively. Each gray line connects Q_{Lg} of Sichuan Basin and Chuan-Dian Block at the same frequency, and by plotting the Q_{Lg} of ELIP core at this frequency, the viscosity of ELIP core can be interpolated.

4.3. Tectonic Model for the SE Tibetan Plateau

In addition to the brittle/viscous crustal flow and the ELIP core interference, the eastward subduction of the Indian Plate plays a crucial role in the crustal deformation in the SE Tibetan Plateau (T. Zheng et al., 2020). South of ~26°N, the SKS splitting analysis observed a sharp change in fast polarization direction from south–north direction in the north to east–west direction, which could be related to the convection within the subducting-related mantle wedge beneath Myanmar (e.g., Z. Huang & Chevrot, 2021). This suggests that Anomaly #2 in our Q_{Lg} model corresponds to the transition in mantle dynamics from an extrusion tectonic to a subduction regime. Dynamic instability may lead to lithospheric delamination. The thinned lithosphere, less than 100 km, was accordingly observed beneath the southern Central Yunnan Block (H. Yang et al., 2017). Extensive anomalies of low seismic velocities within the upper mantle were revealed, indicating associated upwelling of the asthenosphere (Feng et al., 2021; Z. Huang et al., 2019). The hot upwelling is further supported by low P-wave velocities at 410 km depth and by the uplifted topography of the 410-discontinuity (Feng et al., 2021; F. Yang, et al., 2023). Eocene-Oligocene potassic magmatic rocks originated from the partial melting of enriched lithospheric mantle, and ancient K-rich crust was widely distributed in the SE Tibetan Plateau, resulting from upwelling asthenosphere (B. Chen et al., 2017). In addition, the temporal-spatial distributions of magma ages near ~26°N may indicate the migration of the slab tearing (Hou et al., 2024). Combining heat from the upwelling asthenosphere and from the slab window, the crust of the overlying Central Yunnan Block may have been extensively heated, resulting in the observed extreme Lg attenuation. The thermal influx from below could have disrupted the cooling of the Late Permian Emeishan basalts, whereas those at shallower depths cooled more efficiently and attained greater mechanical strength. Therefore, we suggest that crustal flow connectivity varies with depth, consistent with the observed frequency-dependent connectivity within the low-Q_{Lg} anomalies. Furthermore, S. Liu et al. (2022) observed that the high-velocity anomaly beneath the ELIP core weakened with increasing depth, with limited extension above ~30 km. They suggested that viscous crustal flow occurs at greater depths, based on a strong low-velocity anomaly beneath Central Yunnan at 30 km depth. This is consistent with S-wave velocity maps averaged for depth ranges of 10–20, 20–30, and 30–40 km, which represent the upper, middle, and lower crust, respectively (Y. Liu et al., 2023). For the low-velocity anomalies beneath Western Sichuan and Central Yunnan, we can see a progressive connectivity pattern, transitioning from isolated features at shallow depths to weakly connected and finally to merged structures depth increases (Figure 7a). Although the low-velocity anomaly became less significant for 30–40 km depth, S-wave velocity up to 3.7 km/s may still indicatet partial melting could, considering the mafic composition within the crust (C. Li et al., 2024). Seismic attenuation demonstrated that the Q_{Pg} and frequency-dependent Q_{Lg} maps correspond (Figure 7b). Pg-wave is observed at shorter distances than Lg, and at these distances, P-wave tends to be totally reflected by intra-crustal discontinuities. Therefore, the Pg-wave attenuation reflects the whole crustal attenuation characteristics with a larger weight from the upper and middle crust (Campillo et al., 1984; R. J. Li et al., 2023; Sun et al., 2026). R. J. Li et al. (2023) revealed low-Q_{Pg} anomalies in Western Sichuan and Central Yunnan, separated by the pronounced high Q_{Pg} for the ELIP core. By examining the correlation between S-wave velocity and seismic attenuation (Figure S8 in Supporting Information S1), we find that 1.0 Hz Q_{Pg} correlates well with S velocities between 20 and 25 km, whereas for Lg-wave, low-frequency Q_{Lg} correlates better with deeper S velocities. Therefore, we use 1.0 Hz Q_{Pg}, 5.2 and 1.0 Hz Q_{Lg} to indicate attenuation for the upper, middle and lower crust. Such representation cannot rule out effects from scattering, but the expected weaker scattering at lower frequencies (Hoshiba, 1994) is consistent with the increased correlation between low-frequency Q_{Lg} and deeper S velocities. Furthermore, this study does not seek to distinguish between scattering and absorption because they can reflect brittle and viscous

21699356, 2026, 3, Downloaded from https://agupubs.onlinelibrary.wiley.com/doi/10.1029/2025JB032994 by Institution Of Geology, Wiley Online Library on [19/04/2026]. See the Terms and Conditions (https://onlinelibrary.wiley.com/terms-and-conditions) on Wiley Online Library for rules of use; OA articles are governed by the applicable Creative Commons License

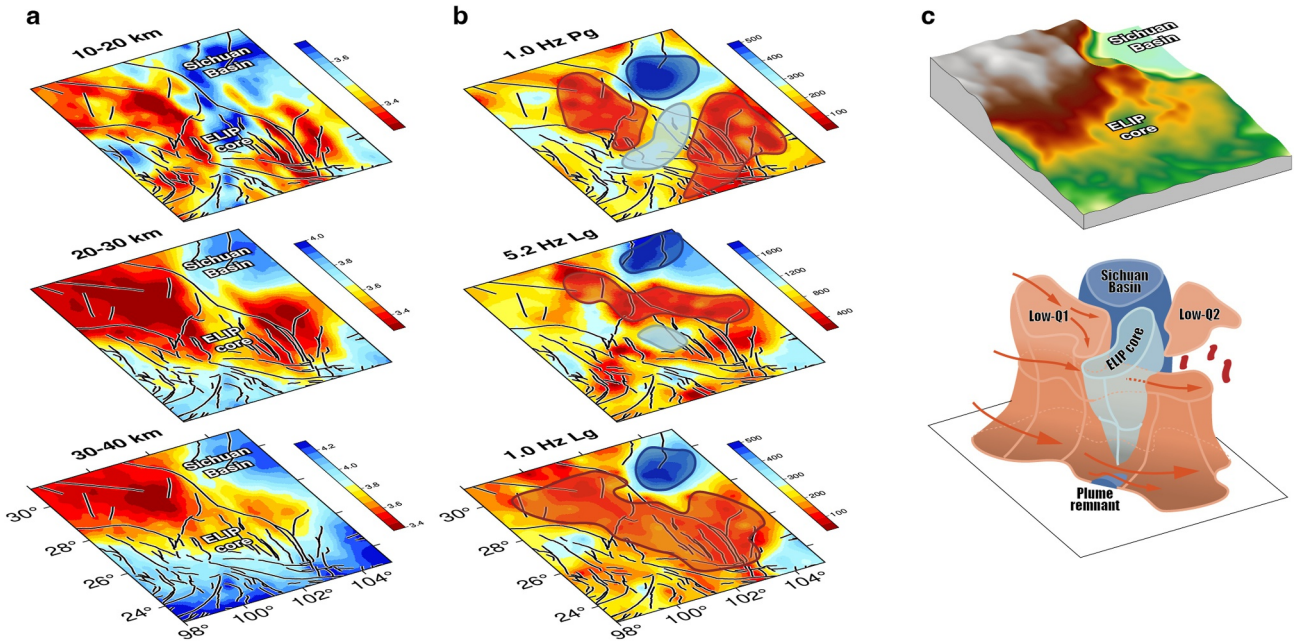

Figure 7. (a) Maps of S-wave velocity (Y. Liu et al., 2023). From top to bottom are velocities averaged for depth ranges of 10–20, 20–30, and 30–40 km. (b) Map of Pg-wave Q at 1.0 Hz (R. J. Li et al., 2023) (top), Lg-wave Q at 5.2 Hz (middle), and 1.0 Hz (bottom). (c) Topography and a cartoon showing the partially connected crustal flow model. The weak crust of the Chuan-Dian block and the rigid Sichuan Basin are shown in orange and blue, respectively. Azure volume represents the Emeishan Large Igneous Province core. Red arrows and red wiggling patches indicate the crustal flow and hot upwelling, respectively.

deformation at shallower and deeper depths, respectively. As the frequency decreases from ~5 to 1 Hz, the low Q_{Lg} values become more widely distributed, indicating a broader distribution of the viscous crust at greater depths. In summary, we proposed the tectonic model of partially connected crustal flow (Figure 7c). In the shallower depths, the cooled and strengthened ELIP core crust impeded the crustal extrusion. As depth increases, the crust of the ELIP core becomes weak due to underlying hot upwelling, allowing viscous crustal flow from Western Sichuan to Central Yunnan. Hot upwelling associated with eastward subduction of the Indian Plate further weakens the Central Yunnan crust, facilitating crustal flow despite partial obstruction of the ELIP core. In summary, under the combined effects of gravitational push and asthenosphere heating, the strengthened ELIP core hindered, though did not completely halt, the crustal flow.

5. Conclusion

We developed a high-resolution broadband Lg-wave attenuation model for the SE Tibetan Plateau. The frequency band is 0.05–10.0 Hz, and the spatial resolution reaches approximately 0.5° × 0.5°. The rigid Sichuan Basin and ancient Laojunshan dome structure features weak Lg attenuation. The Chuan-Dian Block, a significant component of crustal extrusion in the SE Tibetan Plateau, manifests strong Lg attenuation. Significantly low-Q_{Lg} Anomalies #1 and #2 were identified in two subblocks: Western Sichuan and Central Yunnan. In addition to the correspondence of fault activity and low Q_{Lg} at higher frequency bands, low-Q_{Lg} values between ~0.2 and 5 Hz correlated well with low seismic velocities, high conductivity at depths ranging from 20 to 40 km, which suggests the brittle deformation and viscous flow for the shallower and deeper parts of the crust. Our model reveals the high-Q_{Lg} Anomaly #3 in the ELIP core, which is likely related to crustal strengthening by Late Permian magma intrusion. By establishing the relationship between the lateral variations in viscosity and Q_{Lg}, we estimated a viscosity of 6.38×10^{21} Pa · s for the ELIP core with the assigned viscosity of 10^{21} and 10^{24} Pa · s for the Chuan-Dian Block and Sichuan Basin, respectively. Such a strength contrast was expected to produce a limited effect on crustal flow. Restoration tests demonstrated our tomographic model's ability to resolve connectivity within the crustal flow, and the frequency-dependent connectivity between Anomalies #1 and #2 indicates a depth-dependent crustal flow. This is consistent with Pg attenuation and isolated-partially connected-merged anomalies of low S-wave velocity from 10 to 40 km depths. The eastward subduction of the Indian Plate, along with

21699356, 2026, 3, Downloaded from https://agupubs.onlinelibrary.wiley.com/doi/10.1029/2025JB032994 by Institution Of Geology, Wiley Online Library on [19/04/2026]. See the Terms and Conditions (https://onlinelibrary.wiley.com/terms-and-conditions) on Wiley Online Library for rules of use; OA articles are governed by the applicable Creative Commons License

associated lithospheric delamination and asthenosphere upwelling, contributed to the development of crustal flow. Therefore, the crustal flow in the SE Tibetan Plateau was hindered but not halted by the ELIP core.

Conflict of Interest

The authors declare no conflicts of interest relevant to this study.

Data Availability Statement

The waveforms used in this study were collected from the China Earthquake Network Center, the China Earthquake Data Center, and the Incorporated Research Institutions for Seismology Data Management Center. The continuous Lg, pre-event noise, and pre-phase noise waveforms, single- and two-station Lg amplitude data used in this study, and the resulting Lg-wave attenuation model in the SE Tibetan Plateau are available at the World Data Center for Geophysics, Beijing (He et al., 2025). Specific figures were generated using Generic Mapping Tools (Wessel et al., 2019).

Acknowledgments
The comments from Editor F. Niu, Associate Editor, reviewer J. Russell at Syracuse University, and an anonymous reviewer are valuable and significantly improved the manuscript. This research was supported by the National Natural Science Foundation of China (Grants U2139206, 42104055).

References

Aki, K., & Richards, P. G. (2002). *Quantitative seismology, second edition*. University Science Books.
Anderson, D. L. (1966). Earth's viscosity. *Science*, *151*(3708), 321–322. https://doi.org/10.1126/science.151.3708.321
Bai, D. H., Unsworth, M. J., Meju, M. A., Ma, X. B., Teng, J. W., Kong, X. R., et al. (2010). Crustal deformation of the eastern Tibetan plateau revealed by magnetotelluric imaging. *Nature Geoscience*, *3*(5), 358–362. https://doi.org/10.1038/NGEO830
Bao, X., Song, X., Eaton, D. W., Xu, Y., & Chen, H. (2020). Episodic lithospheric deformation in eastern Tibet inferred from seismic anisotropy. *Geophysical Research Letters*, *47*(3), e2019GL085721. https://doi.org/10.1029/2019GL085721
Bao, X. W., Sun, X. X., Xu, M. J., Eaton, D. W., Song, X. D., Wang, L. S., et al. (2015). Two crustal low-velocity channels beneath SE Tibet revealed by joint inversion of Rayleigh wave dispersion and receiver functions. *Earth and Planetary Science Letters*, *415*, 16–24. https://doi.org/10.1016/j.epsl.2015.01.020
Bao, X. Y., Sandvol, E., Chen, Y. S. J., Ni, J., Hearn, T., & Shen, Y. (2012). Azimuthal anisotropy of Lg attenuation in eastern Tibetan Plateau. *Journal of Geophysical Research*, *117*(B10). https://doi.org/10.1029/2012JB009255
Bao, X. Y., Sandvol, E., Ni, J., Hearn, T., Chen, Y. S. J., & Shen, Y. (2011). High resolution regional seismic attenuation tomography in eastern Tibetan Plateau and adjacent regions. *Geophysical Research Letters*, *38*(16). https://doi.org/10.1029/2011GL048012
Boyd, O. S., Jones, C. H., & Sheehan, A. F. (2004). Foundering lithosphere imaged beneath the southern Sierra Nevada, California, USA. *Science*, *305*(5684), 660–662. https://doi.org/10.1126/science.1099181
Campillo, M., Bouchon, M., & Massinon, B. (1984). Theoretical study of the excitation, spectral characteristics, and geometrical attenuation of regional seismic phases. *Bulletin of the Seismological Society of America*, *74*(1), 79–90. https://doi.org/10.1785/bssa0740010079
Chen, B., Long, X., Wilde, S. A., Yuan, C., Wang, Q., Xia, X., & Zhang, Z. (2017). Delamination of lithospheric mantle evidenced by Cenozoic potassic rocks in Yunnan, SW China: A contribution to uplift of the Eastern Tibetan Plateau. *Lithos*, *284–285*, 709–729. https://doi.org/10.1016/j.lithos.2017.05.019
Chen, J., Hu, J., Yang, H., Zhang, X., Wen, L., & Peng, H. (2012). S-wave Q structure of the crust and upper mantle beneath Yunnan from surface waves. *Science China Earth Sciences*, *55*(5), 858–868. https://doi.org/10.1007/s11430-011-4343-6
Chen, Y., & Xie, J. (2017). Resolution, uncertainty and data predictability of tomographic Lg attenuation models—application to Southeastern China. *Geophysical Journal International*, *210*(1), 166–183. https://doi.org/10.1093/gji/ggx147
Cui, T., & Chen, X. (2023). Magnetotelluric imaging and tectonic movement characteristics of the central Yunnan sub-block and its adjacent areas. *Science China Earth Sciences*, *66*(2), 377–392. https://doi.org/10.1007/s11430-021-9997-y
Dai, A., Tang, C.-C., Liu, L., & Xu, R. (2020). Seismic attenuation tomography in southwestern China: Insight into the evolution of crustal flow in the Tibetan Plateau. *Tectonophysics*, *792*, 228589. https://doi.org/10.1016/j.tecto.2020.228589
Ding, L., Kapp, P., Cai, F., Garzione, C. N., Xiong, Z., Wang, H., & Wang, C. (2022). Timing and mechanisms of Tibetan Plateau uplift. *Nature Reviews Earth and Environment*, *3*(10), 652–667. https://doi.org/10.1038/s43017-022-00318-4
Duan, M., Zhou, L., Zhao, C., Liu, Z., & Zhang, X. (2024). High-Resolution 3D QP and QS models of the Middle Eastern boundary of the Sichuan–Yunnan rhombic block: New Insight into implication for seismogenesis. *Seismological Research Letters*, *95*(3), 1759–1775. https://doi.org/10.1785/0220230232
Feng, J., Yao, H., Chen, L., & Wang, W. (2021). Massive lithospheric delamination in southeastern Tibet facilitating continental extrusion. *National Science Review*, *9*(4), nwab174. https://doi.org/10.1093/nsr/nwab174
Fu, Y. V., Jia, R., Han, F., & Chen, A. (2018). SH wave structure of the crust and upper mantle in southeastern margin of the Tibetan Plateau from teleseismic Love wave tomography. *Physics of the Earth and Planetary Interiors*, *279*, 15–20. https://doi.org/10.1016/j.pepi.2018.04.002
Fu, Y. Y. V., Gao, Y., Li, A. B., Li, L., & Chen, A. G. (2017). Lithospheric structure of the southeastern margin of the Tibetan Plateau from Rayleigh wave tomography. *Journal of Geophysical Research*, *122*(6), 4631–4644. https://doi.org/10.1002/2016jb013096
Gan, W., Molnar, P., Zhang, P., Xiao, G., Liang, S., Zhang, K., et al. (2021). Initiation of clockwise rotation and eastward transport of Southeastern Tibet inferred from deflected fault traces and GPS observations. *GSA Bulletin*, *134*(5–6), 1129–1142. https://doi.org/10.1130/b36069.1
Guo, Z., Guan, M., & Chapman, M. C. (2022). Amplification and attenuation due to geologic conditions in the Sichuan Basin, central China. *Seismological Research Letters*, *94*(1), 399–413. https://doi.org/10.1785/0220220030
Han, C., Huang, Z., Hao, S., Wang, L., Xu, M., & Hammond, J. O. S. (2022). Restricted lithospheric extrusion in the SE Tibetan Plateau: Evidence from anisotropic Rayleigh-wave tomography. *Earth and Planetary Science Letters*, *598*, 117837. https://doi.org/10.1016/j.epsl.2022.117837
He, X., Zhao, L.-F., Xie, X.-B., Li, R.-J., Lu, T., & Yao, Z.-X. (2025). Hindered but not Halted Crustal Flow: Implications from Lg-wave Attenuation Tomography based on high-density ChinArray in SE Tibetan Plateau [Dataset]. *World Data Center for Geophysics, Beijing*. http://www.geophys.ac.cn/ArticleDataInfo.asp?MetaId=725

21699356, 2026, 3, Downloaded from https://agupubs.onlinelibrary.wiley.com/doi/10.1029/2025JB032994 by Institution Of Geology, Wiley Online Library on [19/04/2026]. See the Terms and Conditions (https://onlinelibrary.wiley.com/terms-and-conditions) on Wiley Online Library for rules of use; OA articles are governed by the applicable Creative Commons License

He, X., Zhao, L.-F., Xie, X.-B., Tian, X., & Yao, Z.-X. (2021). Weak crust in southeast Tibetan Plateau revealed by Lg-wave attenuation tomography: Implications for crustal material escape. *Journal of Geophysical Research*, *126*(3), e2020JB020748. https://doi.org/10.1029/2020JB020748

Hoshiba, M. (1994). Simulation of coda wave envelope in depth dependent scattering and absorption structure. *Geophysical Research Letters*, *21*(25), 2853–2856. https://doi.org/10.1029/94GL02718

Hou, Z., Liu, L., Zhang, H., Xu, B., Wang, Q., Yang, T., et al. (2024). Cenozoic eastward growth of the Tibetan Plateau controlled by tearing of the Indian slab. *Nature Geoscience*, *17*(3), 255–263. https://doi.org/10.1038/s41561-024-01382-9

Huang, H., Yao, H. J., & van der Hilst, R. D. (2010). Radial anisotropy in the crust of SE Tibet and SW China from ambient noise interferometry. *Geophysical Research Letters*, *37*(21). https://doi.org/10.1029/2010GL044981

Huang, Z., & Chevrot, S. (2021). Mantle dynamics in the SE Tibetan Plateau revealed by teleseismic shear-wave splitting analysis. *Physics of the Earth and Planetary Interiors*, *313*, 106687. https://doi.org/10.1016/j.pepi.2021.106687

Huang, Z., Wang, L., Xu, M., Zhao, D., Mi, N., & Yu, D. (2019). P and S wave tomography beneath the SE Tibetan Plateau: Evidence for lithospheric delamination. *Journal of Geophysical Research*, *124*(10), 10292–10308. https://doi.org/10.1029/2019JB017430

Karato, S.-i. (2010). Rheology of the Earth's mantle: A historical review. *Gondwana Research*, *18*(1), 17–45. https://doi.org/10.1016/j.gr.2010.03.004

Kreemer, C., Blewitt, G., & Klein, E. C. (2014). A geodetic plate motion and Global Strain Rate Model. *Geochemistry, Geophysics, Geosystems*, *15*(10), 3849–3889. https://doi.org/10.1002/2014GC005407

Li, C., Yu, C., Hillenbrand, I., & Zhang, W. (2024). Three-Dimensional crustal channel flows beneath the Southeastern Tibetan Plateau revealed by full-waveform ambient noise tomography. *Geophysical Research Letters*, *51*(22), e2024GL110704. https://doi.org/10.1029/2024GL110704

Li, R.-J., Zhao, L.-F., Xie, X.-B., & Yao, Z.-X. (2023). Crustal deformation in the southeastern margin of the Tibetan Plateau: Insights from broadband Pg-wave attenuation tomography. *Geophysical Journal International*, *235*(3), 2870–2886. https://doi.org/10.1093/gji/ggad404

Li, X., Ma, X., Chen, Y., Xue, S., Varentsov, I. M., & Bai, D. (2020). A plume-modified lithospheric barrier to the southeastward flow of partially molten Tibetan crust inferred from magnetotelluric data. *Earth and Planetary Science Letters*, *548*, 116493. https://doi.org/10.1016/j.epsl.2020.116493

Li, Y., & Gao, Y. (2023). Rigid widths of active block boundary faults and crustal layered anisotropy in the intersection of faults Honghe and Xiaojiang in the SE margin of the Tibetan Plateau. *Geophysical Journal International*, *235*(2), 1504–1518. https://doi.org/10.1093/gji/ggad279

Li, Y., Liu, M., Li, Y., & Chen, L. (2019). Active crustal deformation in southeastern Tibetan Plateau: The kinematics and dynamics. *Earth and Planetary Science Letters*, *523*, 115708. https://doi.org/10.1016/j.epsl.2019.07.010

Liu, B., Zhou, Y., & Yang, G. (2017). Characteristics of isostatic gravity anomaly in Sichuan-Yunnan region, China. *Geodesy and Geodynamics*, *8*(4), 238–245. https://doi.org/10.1016/j.geog.2017.04.002

Liu, H., Pei, S., Liu, W., Xue, X., Li, J., Hua, Q., & Li, L. (2024). Crustal and upper mantle attenuation structure beneath the Southeastern Tibetan Plateau and its implications on Plateau outgrowth. *Journal of Geophysical Research*, *129*(2), e2023JB026977. https://doi.org/10.1029/2023JB026977

Liu, Q. Y., van der Hilst, R. D., Li, Y., Yao, H. J., Chen, J. H., Guo, B., et al. (2014). Eastward expansion of the Tibetan Plateau by crustal flow and strain partitioning across faults. *Nature Geoscience*, *7*(5), 361–365. https://doi.org/10.1038/ngeo2130

Liu, S., Chang, K., Yang, D., Xu, X., Wang, W., Yang, S., & Li, M. (2022). Velocity and azimuthal anisotropy structures beneath the Dianzhong Block and its vicinity, SE Tibetan Plateau, revealed by eikonal equation-based traveltime tomography. *Tectonophysics*, *839*, 229525. https://doi.org/10.1016/j.tecto.2022.229525

Liu, S., Yang, Y., Deng, B., Zhong, Y., Wen, L., Sun, W., et al. (2021). Tectonic evolution of the Sichuan Basin, Southwest China. *Earth-Science Reviews*, *213*, 103470. https://doi.org/10.1016/j.earscirev.2020.103470

Liu, Y., Yao, H., Zhang, H., & Fang, H. (2021). The community velocity model V.1.0 of Southwest China, constructed from joint body- and Surface-Wave Travel-Time Tomography. *Seismological Research Letters*, *92*(5), 2972–2987. https://doi.org/10.1785/0220200318

Liu, Y., Yu, Z., Zhang, Z., Yao, H., Wang, W., Zhang, H., et al. (2023). The high-resolution community velocity model V2.0 of southwest China, constructed by joint body and surface wave tomography of data recorded at temporary dense arrays. *Science China Earth Sciences*, *66*(10), 2368–2385. https://doi.org/10.1007/s11430-022-1161-7

Liu, Z., Cao, S., Dong, Y., Li, W., Cheng, X., Wang, H., & Lyu, M. (2021). Deformation structure and exhumation process of the Laojunshan gneiss dome in southeastern Yunnan of China. *Science China Earth Sciences*, *64*(12), 2190–2216. https://doi.org/10.1007/s11430-021-9804-0

Ma, X., Zhao, L.-F., Xie, X.-B., Chang, X., & Yao, Z.-X. (2023). Warm versus cold crust in the Tien Shan orogenic belt revealed by seismic Lg attenuation tomography. *Geophysical Journal International*, *233*(3), 2142–2154. https://doi.org/10.1093/gji/ggad055

Owens, T. J., & Zandt, G. (1997). Implications of crustal property variations for models of Tibetan plateau evolution. *Nature*, *387*(6628), 37–43. https://doi.org/10.1038/387037a0

Paige, C. C., & Saunders, M. A. (1982). LSQR: An algorithm for sparse linear equations and sparse least squares. *ACM Transactions on Mathematical Software*, *8*(1), 43–71. https://doi.org/10.1145/355984.355989

Pang, Y., Wu, Y., Li, Y., & Chen, C. (2023). The mechanism of the present-day crustal deformation in southeast Tibet: From numerical modelling and geodetic observations. *Geophysical Journal International*, *235*(1), 12–23. https://doi.org/10.1093/gji/ggad200

Qiao, L., Yao, H. J., Lai, Y. C., Huang, B. S., & Zhang, P. (2018). Crustal structure of southwest China and northern Vietnam from ambient noise tomography: Implication for the large-scale material transport model in SE Tibet. *Tectonics*, *37*(5), 1492–1506. https://doi.org/10.1029/2018TC004957

Royden, L. H., Burchfiel, B. C., & van der Hilst, R. D. (2008). The geological evolution of the Tibetan Plateau. *Science*, *321*(5892), 1054–1058. https://doi.org/10.1126/science.1155371

Shearer, P. M. (2009). *Introduction to seismology* (2nd ed.). Cambridge University Press.

Shen, L., Zhao, L.-F., Xie, X.-B., Yang, G., & Yao, Z.-X. (2023). Extremely weak Lg attenuation reveals ancient continental relicts in the South China block. *Earth and Planetary Science Letters*, *611*, 118144. https://doi.org/10.1016/j.epsl.2023.118144

Shi, Y., Duan, L., Meng, Q.-R., Zhan, R., & Wei, R. (2023). Detrital record of sediment influx in the Triassic Chuxiong broken foreland basin in southeastern Tibetan Plateau. *Palaeogeography, Palaeoclimatology, Palaeoecology*, *632*, 111864. https://doi.org/10.1016/j.palaeo.2023.111864

Sun, Q., Pei, S. P., Li, L., Li, J. W., Zhang, C., & Tang, X. G. (2026). Faults and fluids activity controlled structural heterogeneity in the upper crust beneath the Xiaojiang fault system revealed from 2-D Pg seismic tomography. *Geophysical Journal International*, *244*(1), ggaf424. https://doi.org/10.1093/gji/ggaf424

Tang, Z., Yang, D., Pan, W., Dong, X., Wang, N., & Xia, J. (2022). Adjoint attenuation tomography of Sichuan–Yunnan Region. *Seismological Research Letters*, *94*(2A), 898–912. https://doi.org/10.1785/0220220189

21699356, 2026, 3, Downloaded from https://agupubs.onlinelibrary.wiley.com/doi/10.1029/2025JB032994 by Institution Of Geology, Wiley Online Library on [19/04/2026]. See the Terms and Conditions (https://onlinelibrary.wiley.com/terms-and-conditions) on Wiley Online Library for rules of use; OA articles are governed by the applicable Creative Commons License

Tapponnier, P., Zhiqin, X., Roger, F., Meyer, B., Arnaud, N., Wittlinger, G., & Jingsui, Y. (2001). Oblique stepwise rise and growth of the Tibet plateau. *Science*, *294*(5547), 1671–1677. https://doi.org/10.1126/science.105978

Todrani, A., Speranza, F., D'Agostino, N., & Zhang, B. (2022). Post-50 Ma evolution of India-Asia collision Zone from paleomagnetic and GPS data: Greater India indentation to eastward Tibet flow. *Geophysical Research Letters*, *49*(1), e2021GL096623. https://doi.org/10.1029/2021GL096623

Wang, M., & Shen, Z.-K. (2020). Present-Day crustal deformation of Continental China derived from GPS and its tectonic implications. *Journal of Geophysical Research*, *125*(2), e2019JB018774. https://doi.org/10.1029/2019JB018774

Wang, W., Qiao, X., & Ding, K. (2021). Present-Day kinematics in Southeastern Tibet inferred from GPS measurements. *Journal of Geophysical Research*, *126*(1), e2020JB021305. https://doi.org/10.1029/2020JB021305

Wang, W. L., Wu, J. P., Fang, L. H., Lai, G. J., & Cai, Y. (2017). Crustal thickness and Poisson's ratio in southwest China based on data from dense seismic arrays. *Journal of Geophysical Research*, *122*(9), 7219–7235. https://doi.org/10.1002/2017JB013978

Wei, Z., & Zhao, L. (2019). Lg-Q model and its implication on high-frequency ground motion for earthquakes in the Sichuan and Yunnan region. *Earth and Planetary Physics*, *3*, 526–536. https://doi.org/10.26464/epp2019054

Wessel, P., Luis, J. F., Uieda, L., Scharroo, R., Wobbe, F., Smith, W. H. F., & Tian, D. (2019). The generic mapping tools version 6. *Geochemistry, Geophysics, Geosystems*, *20*(11), 5556–5564. https://doi.org/10.1029/2019gc008515

Wu, R.-S., Jin, S., & Xie, X.-B. (2000). Energy partition and attenuation of Lg waves by numerical simulations using screen propagators. *Physics of the Earth and Planetary Interiors*, *120*(3), 227–243. https://doi.org/10.1016/S0031-9201(99)00167-3

Xie, J., Wu, Z., Liu, R., Schaff, D., Liu, Y., & Liang, J. (2006). Tomographic regionalization of crustal Lg Q in eastern Eurasia. *Geophysical Research Letters*, *33*(3). https://doi.org/10.1029/2005GL024410

Xu, M., Huang, Z., Wang, L., Xu, M., Zhang, Y., Mi, N., et al. (2020). Sharp lateral moho variations across the SE Tibetan Margin and their implications for Plateau growth. *Journal of Geophysical Research*, *125*(5), e2019JB018117. https://doi.org/10.1029/2019JB018117

Yamauchi, H., & Takei, Y. (2024). Effect of melt on polycrystal anelasticity. *Journal of Geophysical Research*, *129*(4), e2023JB027738. https://doi.org/10.1029/2023JB027738

Yang, F., Li, J., Chen, S., Chen, Y., Li, L., & Ai, Y. (2023). Intracontinental lithospheric delamination: Constraints from imaging the mantle transition zone beneath the southwestern part of the Sichuan Basin. *Science China Earth Sciences*, *66*(10), 2340–2352. https://doi.org/10.1007/s11430-022-1129-9

Yang, H., Peng, H., & Hu, J. (2017). The lithospheric structure beneath southeast Tibet revealed by P and S receiver functions. *Journal of Asian Earth Sciences*, *138*, 62–71. https://doi.org/10.1016/j.jseaes.2017.02.001

Yang, J., Kaus, B. J. P., Li, Y., Leloup, P. H., Popov, A. A., Lu, G., et al. (2020). Lower crustal rheology controls the development of large offset strike-slip faults during the Himalayan-Tibetan orogeny. *Geophysical Research Letters*, *47*(18), e2020GL089435. https://doi.org/10.1029/2020GL089435

Yang, X., Luo, Y., Jiang, C., Yang, Y., Niu, F., & Li, G. (2023). Crustal and upper Mantle velocity structure of SE Tibet from joint inversion of rayleigh wave phase velocity and teleseismic body wave data. *Journal of Geophysical Research*, *128*(7), e2022JB026162. https://doi.org/10.1029/2022JB026162

Yang, Y. J., Ritzwoller, M. H., Zheng, Y., Shen, W. S., Levshin, A. L., & Xie, Z. J. (2012). A synoptic view of the distribution and connectivity of the mid-crustal low velocity zone beneath Tibet. *Journal of Geophysical Research*, *117*(B4), B04303. https://doi.org/10.1029/2011jb008810

Yin, A., & Harrison, T. M. (2000). Geologic evolution of the Himalayan-Tibetan orogen. *Annual Review of Earth and Planetary Sciences*, *28*(1), 211–280. https://doi.org/10.1146/annurev.earth.28.1.211

Zhang, L., Zhao, L.-F., Xie, X.-B., Wu, Q.-J., & Yao, Z.-X. (2022). Lateral variations in crustal Lg attenuation in and around the Hangay Dome, Mongolia. *International Journal of Earth Sciences*, *111*(2), 591–606. https://doi.org/10.1007/s00531-021-02131-8

Zhang, Z., Yao, H., & Yang, Y. (2020). Shear wave velocity structure of the crust and upper mantle in Southeastern Tibet and its geodynamic implications. *Science China Earth Sciences*, *63*(9), 1278–1293. https://doi.org/10.1007/s11430-020-9625-3

Zhao, L. F., Xie, X. B., He, J. K., Tian, X. B., & Yao, Z. X. (2013). Crustal flow pattern beneath the Tibetan Plateau constrained by regional Lg-wave Q tomography. *Earth and Planetary Science Letters*, *383*, 113–122. https://doi.org/10.1016/j.epsl.2013.09.038

Zhao, L. F., Xie, X. B., Wang, W. M., Zhang, J. H., & Yao, Z. X. (2013). Crustal Lg attenuation within the North China Craton and its surrounding regions. *Geophysical Journal International*, *195*(1), 513–531. https://doi.org/10.1093/gji/ggt235

Zhao, S., Yao, H., Feng, J., & Liu, Y. (2024). Continental extrusion and laterally heterogeneous deformation characteristics within Southeast Tibet. *Tectonics*, *43*(12), e2024TC008438. https://doi.org/10.1029/2024TC008438

Zheng, C., Zhang, R., Wu, Q., Li, Y., Zhang, F., Shi, K., & Ding, Z. (2019). Variations in crustal and uppermost mantle structures across Eastern Tibet and adjacent regions: Implications of crustal flow and asthenospheric upwelling combined for expansions of the Tibetan Plateau. *Tectonics*, *38*(8), 3167–3181. https://doi.org/10.1029/2018TC005276

Zheng, G., Wang, H., Wright, T. J., Lou, Y., Zhang, R., Zhang, W., et al. (2017). Crustal deformation in the India-Eurasia collision zone from 25 years of GPS measurements. *Journal of Geophysical Research*, *122*(11), 9290–9312. https://doi.org/10.1002/2017JB014465

Zheng, T., He, Y., Ding, L., Jiang, M., Ai, Y., Mon, C. T., et al. (2020). Direct structural evidence of Indian continental subduction beneath Myanmar. *Nature Communications*, *11*(1), 1944. https://doi.org/10.1038/s41467-020-15746-3

Zheng, X. F., Yao, Z. X., Liang, J. H., & Zheng, J. (2010). The role played and opportunities provided by IGP DMC of China National Seismic Network in Wenchuan earthquake disaster relief and researches. *Bulletin of the Seismological Society of America*, *100*(5B), 2866–2872. https://doi.org/10.1785/0120090257

Zhou, L., Song, X., Yang, X., & Zhao, C. (2020). Rayleigh wave attenuation tomography in the crust of the Chinese mainland. *Geochemistry, Geophysics, Geosystems*, *21*(8), e2020GC008971. https://doi.org/10.1029/2020GC008971

Zhou, L. Q., Zhao, C. P., Xiu, J. G., & Chen, Z. L. (2008). Tomography of Q(Lg) in Sichuan-Yunnan zone. *Chinese Journal of Geophysics*, *51*, 1745–1752.

21699356, 2026, 3, Downloaded from https://agupubs.onlinelibrary.wiley.com/doi/10.1029/2025JB032994 by Institution Of Geology, Wiley Online Library on [19/04/2026]. See the Terms and Conditions (https://onlinelibrary.wiley.com/terms-and-conditions) on Wiley Online Library for rules of use; OA articles are governed by the applicable Creative Commons License